

# Simulations of splashing high and low viscosity droplets

Arnout M.P. Boelens<sup>1, a)</sup> and Juan J. de Pablo<sup>2</sup>

<sup>1)</sup>*Department of Energy Resources Engineering, Stanford University, 367 Panama Street, Stanford, California 94305, USA*

<sup>2)</sup>*Institute for Molecular Engineering, The University of Chicago, 5801 South Ellis Avenue, Chicago, Illinois 60637, USA*

(Dated: July 23, 2018)

In this work simulations are presented of low viscosity ethanol and high viscosity silicone oil droplets impacting on a dry solid surface at atmospheric and reduced ambient pressure. The simulations are able to capture both the effect of the ambient gas pressure and liquid viscosity on droplet impact and breakup. The results suggest that the early time droplet impact and gas film behavior for both low and high viscosity liquids share the same physics. However, for later time liquid sheet formation and breakup high and low viscosity liquids behave differently. These results explain why for both kinds of liquids the pressure effect can be observed, while at the same time different high and low viscosity splashing regimes have been identified experimentally.

## I. INTRODUCTION

A high and a low viscosity splash on a dry solid surface look rather different. For low viscosity liquids a corona splash is commonly observed<sup>1</sup>, while high viscosity liquids initially seem to spread smoothly over the surface before eventually also breaking up<sup>2</sup>. However, despite these apparent differences, when the ambient gas pressure is reduced splashing is suppressed for both high and low viscosity liquids<sup>3</sup>. This suggests that there is common physics behind both types of splashes. This work explores what the difference between high and low viscosity splashes tells us about splashing in general, and more specifically about the effect of the ambient pressure on splashing.

The question of whether high and low viscosity splashes share the same physics is directly relevant to experimental work on splashing. Because of the very short time scales at which low viscosity splashes occur, from an experimental point of view it is beneficial to work with high viscosity liquids and have the physics of splashing play out in slow motion. For this approach to be valid it is important to know whether results from low and high viscosity splashes can be compared directly. For computer simulations of splashing the reverse case can be made. Due to the computational cost associated with the long time scales of a high viscosity splash it is much more convenient to simulate a low viscosity splash. The simulation of a low viscosity ethanol splash takes on the order of several weeks while a simulation of a high viscosity silicone oil splash takes several months.

Apart from viscosity there are many more parameters that affect the outcome of a droplet impacting on a solid surface. These include impact velocity, droplet diameter, surface tension, and surface roughness<sup>1,4</sup>. Despite this wide range of parameters, the effect of a reduction of the ambient gas pressure is the same: splashing is suppressed<sup>2</sup>. There are various theories that aim to describe droplet impact and the pressure effect. Mongruel *et al.*<sup>5</sup> propose that the characteristic time and length scale of the onset of splashing is determined by a balance between inertial and viscous forces. On the other hand, Mandre, Mani, and Brenner<sup>6</sup> derive that in the case of an inviscid liquid a droplet initially skates on a very thin gas film and that the onset of splashing depends on a combination of the viscosity of this gas film and the parameters of the droplet impact. According to Riboux and Gordillo<sup>7,8,9</sup> whether a droplet splashes depends on the balance between a lift force

---

<sup>a)</sup>Electronic mail: boelens@stanford.edu

acting on the liquid and the growth rate of the rim at the edge of the droplet. Liu, Tan, and Xu<sup>10</sup> attribute splashing to a Kelvin-Helmholtz instability of the gas film under the droplet, and lastly, Sprittles<sup>11</sup> proposes that in the subcontinuum conditions present in the very thin gas film under the droplet a contact line moves faster at reduced ambient gas pressure, causing the gas film to close/collapse earlier at low pressure.

While, none of the above models considers a different high and low viscosity splashing regime, there is experimental evidence that two different regimes exist<sup>2,12,13</sup>. When plotting the ambient threshold pressure, above which splashing can be observed, as function of the viscosity of the liquid two distinct regimes can be observed; for low viscosities the threshold pressure decreases with increasing viscosity while this trend is reversed for higher viscosities<sup>2,12,13</sup>. In this work computer simulations are presented for ethanol and silicone oil droplets impacting a dry solid surface at both atmospheric and reduced ambient pressure. Comparing these two high and low viscosity liquids it is found that the initial deposition stage for high and low viscosity liquids is the same, which explains why for both kinds of liquids the pressure effect can be observed. However, at later times the mechanism for the breakup of the droplet is significantly different. This is consistent with the experimental observation of two different splashing regimes.

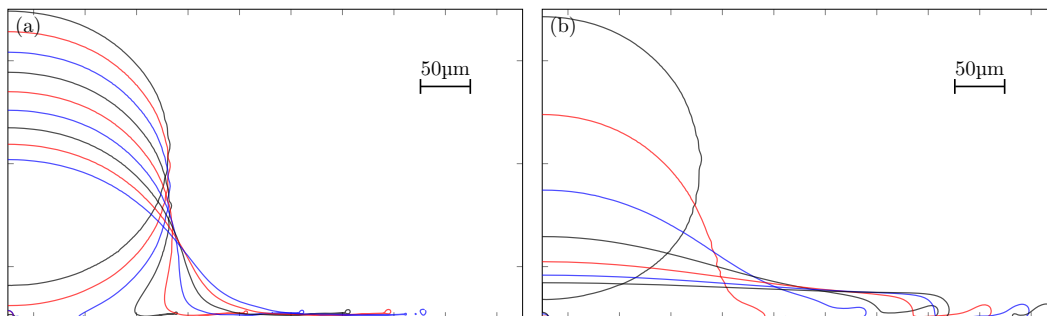


Figure 1. Time series of the interface ( $\alpha = 0.5$ ) of a low viscosity ethanol droplet (a) and a high viscosity silicone oil droplet (b) impacting and spreading on a dry solid surface at atmospheric ambient pressure. Different colors are used to be able to distinguish more clearly between successive contour lines. The time difference between successive lines is  $\Delta t/\tau = 0.0667$  for the ethanol droplet (a) and  $\Delta t/\tau = 0.333$  for the silicone oil droplet (b). Comparing both droplets shows that the characteristic time scale for deposition, spreading, and breakup is much longer for the high viscosity silicone oil than for the low viscosity ethanol.

## II. THEORY & METHOD

To be able to capture both the effect of the liquid viscosity and the ambient gas pressure on impact, spreading, and breakup of the different droplets, the simulations use a finite volume implementation of the Volume Of Fluid (VOF) method<sup>14</sup>. The VOF approach evolves around the definition of a phase parameter  $\alpha$  with the following properties:

$$\alpha = \begin{cases} 0 & \text{in gas phase} \\ (0, 1) & \text{on interface} \\ 1 & \text{in liquid phase} \end{cases} \quad (1)$$

The evolution of  $\alpha$  is calculated using the following transport equation:

$$\frac{\partial \alpha}{\partial t} + \nabla \cdot (\alpha \vec{v}) + \nabla \cdot (\alpha(1 - \alpha) \vec{v}_{lg}) = 0, \quad (2)$$

where  $\vec{v}$  is the phase averaged velocity, and  $\vec{v}_{lg}$  is a velocity field suitable to compress the interface. This equation is equivalent to a material derivative, but rewritten to minimize numerical diffusion<sup>15</sup>.

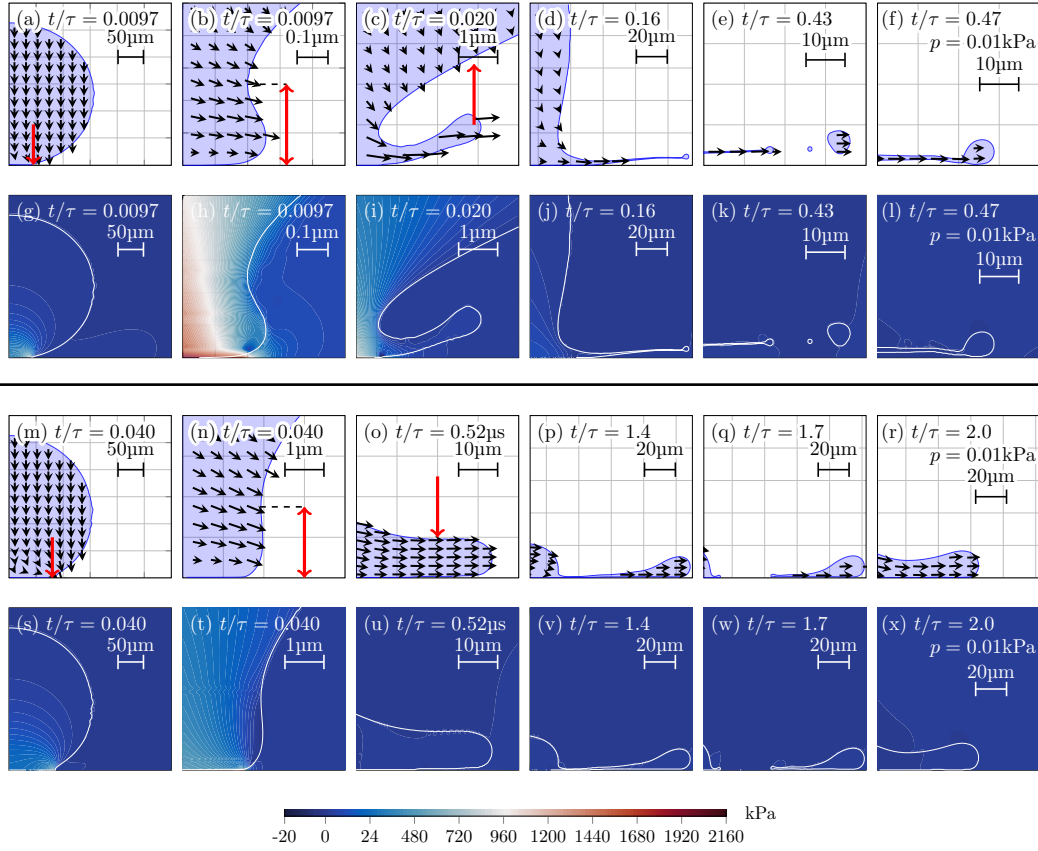


Figure 2. Time series of the impact of low viscosity ethanol droplets (a–l) and high viscosity silicone oil droplets (m–x). In (a–f) and (m–r) blue depicts the liquid phase and white the gas phase. The black arrows depict the direction of the velocity vector field of the liquid phase. Images (g–l) and (s–x) show the pressure field (in kPa). All the images of the pressure field are shown at the same times as the vector plots. (a and g) Cross section of the whole ethanol droplet at the moment of lamella formation. The red arrow in image (a) indicates the position of the contact line. (b and h) Magnified depiction of the contact line at the moment of lamella formation. The height of the lamella is on the order of  $0.1\mu\text{m}$ . (c and i) Because the lamella is very thin and travels at high speed it gets vertically ejected right after impact as a liquid sheet. (d and j) The liquid sheet continues to travel through the air till it breaks up at the rim in images (e) and (k). (f and l) At reduced ambient gas pressure the liquid sheet does not get broken up and splashing is suppressed. (m and s) Cross section of the silicone oil droplet at the moment of lamella formation. The red arrow indicates the position of contact line. (n and t) Magnified depiction of the contact line at the moment of lamella formation. The height of the lamella is on the order of  $1.0\mu\text{m}$ . (o and u) Because the lamella is very thick it continues spreading horizontally till it eventually starts thinning out at the position of the red arrow and a liquid sheet is formed in images (p) and (v). (q and w) At atmospheric pressure the liquid sheet breaks up while at reduced pressure the splash is suppressed in images (r) and (x). The time series show that both the effect of ambient gas pressure and liquid viscosity is captured in the simulations. The observed high pressures regions are associated with gas escaping from under the droplet upon impact and gas film collapse under the droplet. There are no high pressure peaks associated with the spreading and breakup of the liquid sheet. Right after breakup in images (e) and (k) the liquid sheet thickness is about 6 grid cells.

The phase parameter is used to calculate the phase averaged density,  $\rho$ , velocity,  $\vec{v}$ , and viscosity,  $\mu$ , which are used in the momentum balance:

$$\frac{\partial \rho \vec{v}}{\partial t} + \nabla \cdot (\rho \vec{v} \otimes \vec{v}) = -\nabla p + \nabla \cdot (\mu \nabla \vec{v}) + \rho \vec{g} - \vec{f}, \quad (3)$$

and the continuity equation:

$$\nabla \cdot \vec{v} = 0. \quad (4)$$

In the above equations  $t$  is time,  $p$  is pressure,  $g$  is gravity,  $\vec{f}$  is any body force, like the surface tension force, and  $\otimes$  is the dyadic product. To complete the VOF model, an expression is needed to calculate the surface tension force  $\vec{f}_{\text{st}}$ , and a model is needed for the contact line. The surface tension force is calculated using the expression<sup>16</sup>:

$$\vec{f}_{\text{st}} = \sigma_{\text{st}} \kappa \nabla \alpha \quad (5)$$

where  $\sigma_{\text{st}}$  is the surface tension coefficient, and  $\kappa$  is the curvature of the interface.

The effect of varying the Young's angle  $\theta_0$  from  $0^\circ$  to  $180^\circ$  is calculated directly through the Generalized Navier Boundary Condition (GNBC) at the impact wall<sup>17,18</sup>. With this boundary condition the dynamic contact angle  $\theta$  is allowed to vary freely, but a restoring line-tension force is applied at the contact line whenever the dynamic angle deviates from  $\theta_0$ . This restoring force is an additional source term in the Navier-Stokes equations, and has the following form:

$$\vec{f}_{\text{lt}} = -\frac{\sigma_{\text{st}}}{h} \cos \theta_0 \nabla_{2\text{D}} \alpha \quad (6)$$

In the above equation  $\sigma_{\text{st}}$  is the surface tension coefficient,  $h$  is the height of the local grid cell, and  $\nabla_{2\text{D}} \alpha$  is the gradient of  $\alpha$  on the wall. This force is applied on the liquid-gas interface in the first grid cells adjacent to the wall and is balanced by the surface tension force when  $\theta$  is equal to  $\theta_0$ . Away from the contact line the used implementation of the generalized Navier boundary condition reduces to the Navier-slip boundary condition. Using this slip boundary condition gives a good approximation for the thin film behavior at the wall<sup>11,19</sup>. Because the model used can accommodate only one value for the slip length, a value of  $\lambda = 1\text{nm}$  is chosen to be able to accurately describe the contact line. However, in practice the effective slip length is on the order of the mesh size of  $10\text{nm}$ <sup>20</sup>. This results in the gas film potentially closing faster in our simulations than if the slip length were truly  $1\text{nm}$ .

Table I. An overview of the non-dimensional numbers and ratios of liquid and gas properties at atmospheric pressure. For the simulations at reduced pressure the dynamic viscosity is kept constant, but the kinematic viscosity and gas density are allowed to change.

	Re	We	$\rho_l/\rho_g$	$\nu_l/\nu_g$
Ethanol	1973	1057	789	0.1028
Silicone oil	281	1396	935	0.7226

The simulations are performed for ethanol and silicone oil in air using the VOF solver of the OpenFOAM Finite Volume toolbox<sup>21</sup> at up to  $10\text{nm}$  resolution at the wall. Complete convergence at the contact line would require a grid size below the slip length, which is beyond the reach of our computational resources. Nevertheless, at a grid size of  $10\text{nm}$  the necessary physics of splashing are already present, and we expect the main observations of our simulations to be qualitatively correct<sup>22</sup>. To reduce memory requirements, the simulations are performed in a 2-D axisymmetric geometry and the droplets have a diameter of  $300\mu\text{m}$ . This results in the non-dimensional numbers shown in Tab. I. The Reynolds number is defined as:  $\text{Re} = V_0 D/\nu_l$ , and the Weber number as:  $\text{We} = \rho_l V_0^2 D/\sigma$ . The

material properties of ethanol and silicone oil were chosen because these liquids have been used in many experiments<sup>2,3,12,13</sup> and because the defining difference between them is their viscosity. For the simulations at reduced ambient gas pressure the density of the gas phase is reduced 100 times while keeping the dynamic viscosity constant<sup>23</sup>. This value is well below the ambient pressure threshold typically observed in experiments<sup>3</sup> to make sure the simulations are performed well into the suppressed splashing regime. More information on the boundary conditions at the contact line can be found in Ref. 24. More information on the equations, initial conditions, and a comparison with experiments can be found in Ref. 22. A direct comparison between simulations and experiments is very challenging because the simulations cannot be scaled up due to computational costs and the experiments are hard to scale down due to the difficulties of imaging micro meter scale droplets<sup>25</sup>. However, in this paper an indirect comparison is performed and it is shown that the scaling of the gas film height as function of impact velocity is consistent with theory and experiments. Also, multiple experimental observations are reproduced, including the formation of the central air bubble, liquid sheet formation, and contact line instability<sup>22</sup>.

### III. RESULTS

Unless mentioned otherwise, all units are made dimensionless using the impact velocity  $V_0$  and droplet diameter  $D$ . This results in an inertial time scale:  $\tau = D/V_0 = 30\mu\text{s}$ . As a droplet spreads over a surface, two different gas films are observed under the droplet; initially at the edge of the droplet a very thin gas film is present, on the order of 10nm thick<sup>6,22,26</sup>. When the liquid spreads on top of this gas film in a rolling motion<sup>27,28</sup> or when there is a 3 phase contact line present this is called a lamella. When the liquid spreads on a gas film which is on the order of several  $\mu\text{m}$  thick<sup>13,22</sup> or when the liquid gets lifted up in the air completely this is called a liquid sheet. At the resolution used in this work the gas film on the order of 10nm is under-resolved. However, in previous work it was shown that as long as the gas film is present all the essential features of splashing are captured<sup>22</sup>.

To illustrate the difference between a low and high viscosity splash, Fig. 1 shows a time series of the interface of both a simulated ethanol droplet (a) and a simulated silicone oil droplet (b) splashing at atmospheric ambient pressure. Different colors are used to improve readability of the plots. In Fig. 1 (a) the time difference between two curves is  $\Delta t/\tau = 0.0667$  and in Fig. 1 (b) the time difference is  $\Delta t/\tau = 0.333$ . A first observation that can be made by comparing both time series is how much longer the silicone oil droplet takes to splash than the ethanol droplet. Also, the lamella and subsequent liquid sheet formed in the ethanol splash appears to be much thinner than the lamella formed in the silicone oil splash, which is consistent with literature<sup>5</sup>. On the other hand, the typical crown splash observed in experiments when an ethanol droplet impacts on a solid dry wall is not observed in the simulations. This could be caused by the fact that the droplets used in these simulations are much smaller than a typical droplet used in experiments resulting in a smaller liquid sheet and thus smaller lift force acting on the liquid<sup>22</sup>. To further investigate this difference between the experimental and simulation results, a closer look is taken at the simulations in Fig. 2.

Fig. 2 shows a time series of the impact of low viscosity ethanol droplets (a-l) and high viscosity silicone oil droplets (m-x). In the images (a-f) and (m-r) the liquid phase is blue and the gas phase is white. The black arrows show the direction of the velocity vector field inside the liquid. In addition to the direction of the velocity vector field, Figs. 2 (g-l) and (s-x) show the pressure field at the same times and locations as the vector field. Figs. 2 (a) and (g) show the whole ethanol droplet at the moment a lamella can first be detected at atmospheric ambient pressure. Subsequent images are zoomed in at the contact line, where the red arrow is pointing in Fig. 2 (a). Figs. 2 (m) and (s) also shows the whole droplet at the moment of lamella ejection, but for silicone oil. Comparing Figs. 2 (a) and (g) with Figs. 2 (m) and (s) shows again that the dynamics are much slower for high viscosity liquids and that for silicone oil the lamella forms much later than for ethanol. In

Figs. 2 (b) and (h) and Figs. 2 (n) and (t) both droplets are shown at the same times as in Figs. (a) and (g) and Fig. (m) and (s), but zoomed in at the contact line. The shape of the droplets looks very similar, but the characteristic length scale of the lamella is much larger for silicone oil than ethanol. This is consistent with literature that proposes self-similarity solutions to describe the interface of the spreading droplets<sup>27</sup>. As the droplets approach the surface a large pressure build up can be observed at the stagnation point. This causes the droplet to deform and a new high pressure region forms away from the center where the ambient gas is escaping from under the droplet at high speed. This high pressure area is still present at the time of lamella ejection in Figs. 2 (g) and (h). In Fig. 2 (t) also a higher pressure can be observed at the interface under the droplet. This is caused by the break down of the gas film under the droplet into small gas bubbles. This causes high local curvature of the interface and corresponding regions of high Laplace pressure. In the case of the ethanol droplet a thicker gas film forms right away at the edge of the lamella, turning it into a liquid sheet. In addition, this liquid sheet gets ejected with a strong vertical component, similarly to the behavior observed in a crown splash. For the silicone oil droplet the lamella continues to spread horizontally till eventually the lamella starts thinning out. This is shown in Figs. 2 (o) and (u) where the red arrow indicates the location where a minimum in the interface is first observed. Figs. 2 (d) and (j) show the ethanol liquid sheet continuing to travel through the air till eventually the sheet breaks up at the edge of the rim in Figs. 2 (e) and (k). The silicone oil lamella meanwhile continues to thin out and a thicker air film is entrained under the lamella, turning it into a liquid sheet in Figs. 2 (p) and (v). In Figs. 2 (q) and (w) the silicone oil liquid sheet breaks up. However, in this case the sheet breaks up at the lamella side and not at the rim, suggesting a different breakup mechanism. Figs. 2 (f) and (l) and Figs. 2 (r) and (x) show the ethanol and silicone oil liquid sheet staying intact and not breaking up in the case of simulations with a reduced ambient gas pressure. As can be seen in Figs. 2 (j-l) and Figs. 2 (u-x), there are no high pressure regions observed associated with the spreading of the lamella and liquid sheet breakup.

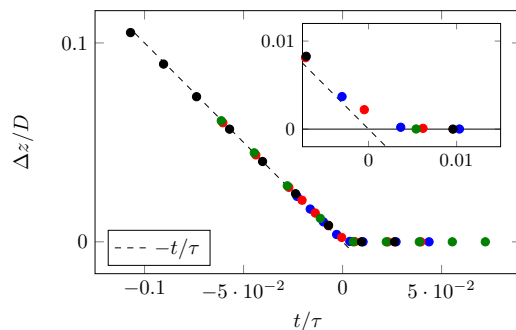


Figure 3. The height between the bottom of the droplet and the surface,  $\Delta z$ , as function of time,  $t$ , for silicone oil at reduced ambient pressure ( $\bullet$ ), silicone oil at normal ambient pressure ( $\bullet$ ), ethanol at reduced ambient pressure ( $\bullet$ ), and ethanol at normal ambient pressure ( $\bullet$ ). Impact time,  $t = 0$ , is defined as the moment the droplet would have hit the surface if no gas film formed under the droplet. This trajectory is described by the line  $\Delta z/D = -t/\tau$ . The inset shows the deviation from the impact trajectory due to gas film formation.

When a droplet impacts a solid wall initially a thin gas film forms under the droplet, preventing the liquid from touching down on the surface<sup>6,22,26</sup>. Therefore the moment that liquid can first be detected on the wall is not a good definition for the moment of impact. Instead, the height between the bottom of the droplet and the wall,  $\Delta z$ , is plotted as a function of time,  $t$ , and a straight line is fitted to the trajectory of the droplet right before impact. As can be seen in Fig. 3, impact time,  $t = 0$ , is then defined as the moment the droplet would have hit the wall if the gas film under the droplet did not form. The inset shows the deviation from the impact trajectory due to gas film formation.

After impact the droplet spreads over the surface and, when the impact velocity is high

enough, eventually a lamella forms. According to Mongruel *et al.*<sup>5</sup> for low surface tension liquids the moment of lamella formation and the thickness of the lamella are determined by the balance between inertial and viscous forces. The inset in Fig. 4 (a) shows some of the different length scales identified by Mongruel *et al.*<sup>5</sup> which are also used in this work:  $r_c$ , and  $z_c$  are the radial position and height, respectively, of the cusp which forms as the droplet spreads over the surface. This cusp is defined as the minimum of the interface in the radial direction.  $r_l$ , and  $z_l$  show the radial position and height of the lamella. This position is defined by the maximum of the interface in the radial direction. At the moment of lamella formation  $r_c \approx r_l$  and  $z_c \approx z_l$ , and at early times the height  $z_l$  is the characteristic length scale of the lamella. However, in the case of ethanol, at later times when the liquid sheet is ejected into the air,  $z_l$  is a measure of how high the liquid sheet travels above the surface.  $r_{cl}$  is the radial position of the contact line.

The characteristic length scale for the impact regime is the diameter of the droplet, and thus the corresponding Reynolds number is large. As a result the impact regime is dominated by inertia and, because of geometrical considerations, the spreading radius of a droplet scales as:  $r_{cl}/D \propto \sqrt{t/\tau}$ <sup>29</sup>. Fig. 4 (a) shows the spreading radius of the ethanol and silicone oil droplets at both atmospheric and reduced ambient pressure as function of time. The observed scaling is consistent with literature<sup>5,29</sup>. The radial position of the cusp is shown in Fig. 4 (b). Because the location of the cusp closely follows a trajectory on the original spherical interface of the impacting droplet, the position of the cusp also scales with inertia. The relation  $r_c/D = 1.4(t/\tau)^{1/2}$  is proposed by Mongruel *et al.*<sup>5</sup> and is consistent with the simulation results.

On the other hand, the height of a lamella,  $z_l$ , is a very small length scale resulting in a small Reynolds number and flow being dominated by viscous forces. Fig. 4 (c) shows the evolution of the lamella height,  $z_l$ , as function of time,  $t$ , for both ethanol and silicone oil. In the case of an ethanol droplet, right after the lamella is ejected it is lifted up in the air and  $z_l$  increases accordingly. However, when the appropriate scaling is chosen, at the moment of lamella formation the data for both liquids should collapse. Considering the difference between the lamella height for ethanol and silicone oil,  $\Delta z_l$ , it can be observed that the lamella height does indeed not scale with inertia. On the other hand, when viscous scaling is applied in Fig. 4 (d) the data collapses for the moment of lamella ejection and the height of the lamella for both liquids is of the same order. The balance between inertial and viscous forces determines the time of lamella ejection and Fig. 4 (e) shows that increasing the viscosity of the liquid delays the time of lamella ejection,  $\Delta t$ , significantly. By applying the scaling proposed by Mongruel *et al.*<sup>5</sup> which takes into account both inertial and viscous forces the data can be made to collapse. In Fig. 4 (f) the time of lamella ejection is on the same order for both ethanol and silicone oil. Apart from scaling considerations, another feature that can be observed in both Fig. 4 (c) and Fig. 4 (d) is that the ambient gas pressure affects the height of the lamella,  $z_l$ . In the case of ethanol this is a difference in the height at which the lamella travels above the surface, which has been proposed as an explanation for the pressure effect<sup>7,22</sup>. For the silicone oil simulations the height difference is mostly caused by a difference in the shape of the lamella/liquid sheet. This difference in shape is now further explored.

In addition to decreasing the gas film thickness under the liquid sheet, lowering of the ambient gas pressure also affects the position of the contact line,  $r_{cl}$ , and the position of the edge of the droplet/lamella,  $r_l$ . These two effects combined result in a smaller surface area,  $A_s = \pi (r_l^2 - r_{cl}^2)$ , being covered by the liquid sheet. While this effect is very small for the ethanol droplets, for the simulations of silicone oil droplets this effect is quite pronounced, as can be seen in Fig. 5 (b). The difference in the area covered by the liquid sheet also causes the volume of the liquid sheet,  $V_s$ , to be different. This volume is defined as the space occupied by the liquid between the contact line and the edge of the droplet/lamella:  $r_{cl} > r > r_l$ . For ethanol the volume of the liquid sheet does not depend on the pressure. However, Fig. 5 (a) shows that there is a clear difference for the silicone oil simulations. Initially there is a larger liquid volume present in the liquid sheet at atmospheric ambient pressure. At later times the inflow of liquid is greatly reduced. This is partly because there

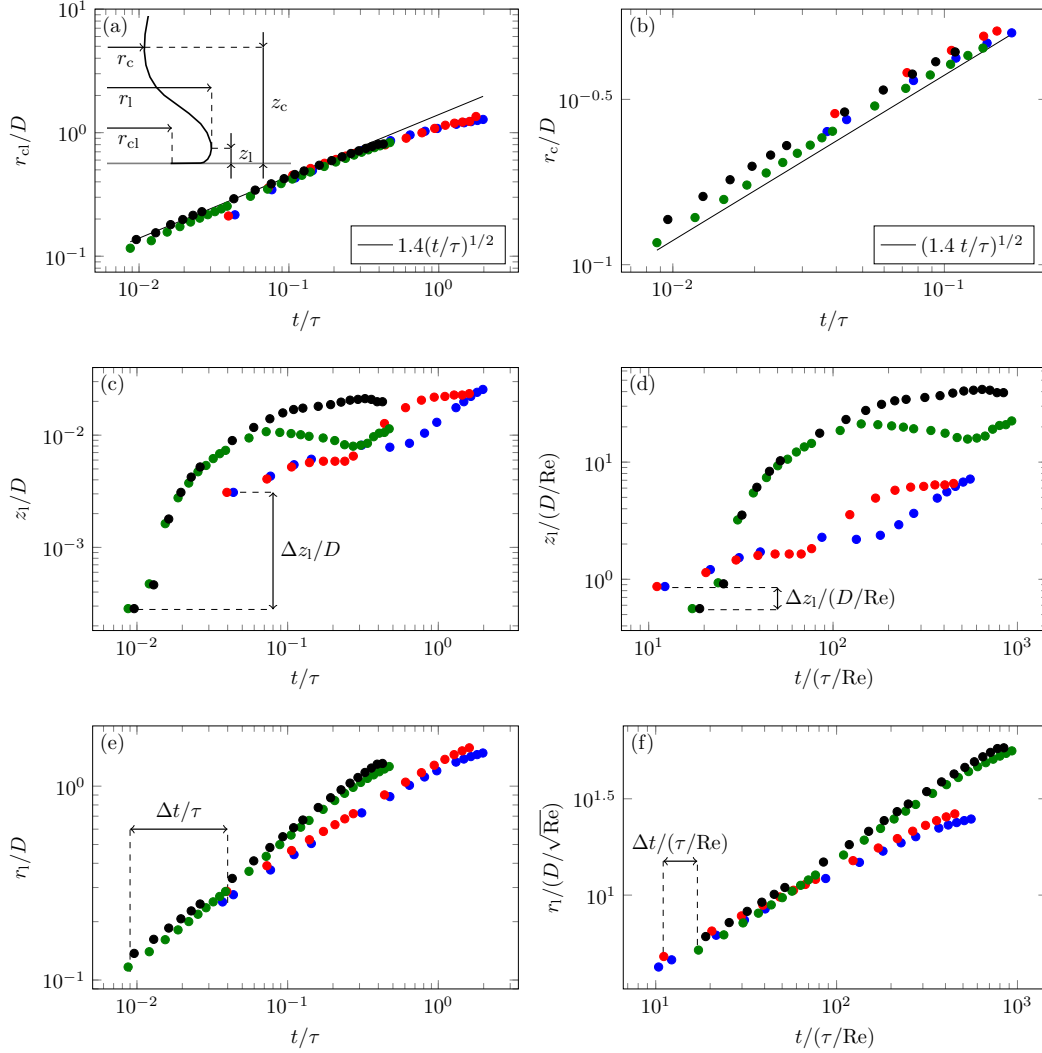


Figure 4. The insert in frame (a) shows a schematic drawing of the parameters referred to in the main text.  $r_c$ , and  $z_c$  are the radial position and height, respectively, of the cusp which forms as the droplet spreads over the surface.  $r_{cl}$  is the radial position of the contact line, and  $r_1$ , and  $z_1$  show the radial position and height of the lamella, respectively. (a) The radial position of the contact line,  $r_{cl}$ , as function of time for (●) silicone oil at reduced ambient pressure, (●) silicone oil at atmospheric ambient pressure, (●) ethanol at reduced ambient pressure, and (●) ethanol at atmospheric ambient pressure. (b) The radial position of the cusp,  $r_c$ , as function of time. (c) The height of the lamella/liquid sheet,  $z_1$ , as function of time using inertial scaling. (d) The height of the lamella/liquid sheet,  $z_1$ , as function of time using viscous scaling. (e) The radial position of the lamella,  $r_1$ , as function of time using inertial scaling. (f) The radial position of the lamella,  $r_1$ , as function of time using mixed scaling. The theoretical curves in both image (a) and (b) are proposed by Mongruel *et al.*<sup>5</sup>, and show that both length scales scale with inertia. When using inertial scaling in image (c) no collapse of the data can be observed. However, When viscous scaling is applied in image (d) at early times the lamella thickness for ethanol and silicone oil becomes of the same order. When applying inertial scaling in image (e) a large time delay can be observed between the moment that the lamella can first be detected in the case of the low viscosity ethanol and the high viscosity silicone oil. When applying the scaling suggested by Mongruel *et al.*<sup>5</sup> in image (f) this time delay is greatly reduced. The error bars in this figure are smaller than the symbols.



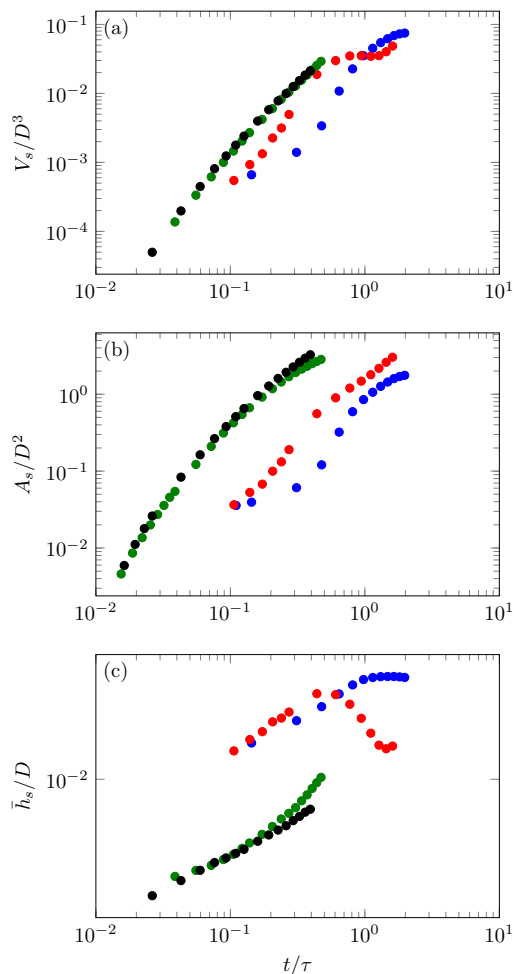


Figure 5. (a) The volume occupied by the liquid in the liquid sheet for (●) silicone oil at low ambient pressure, (●) silicone oil at normal ambient pressure, (●) ethanol at low ambient pressure, and (●) ethanol at normal ambient pressure. The influx of liquid for the silicone oil liquid sheet at atmospheric ambient pressure is initially larger than at reduced ambient pressure. However, later in time a significant reduction can be observed. (b) The surface area covered on the wall by the liquid sheet. Because the contact line moves faster at reduced ambient pressure the surface area covered by the liquid sheet is smaller for both ethanol and silicone oil. (c) The average height of the liquid sheet drops significantly for silicone oil at atmospheric ambient pressure. This causes the liquid sheet to break up. These dynamics are not present for ethanol.

is a positive feedback loop for the average liquid sheet thickness,  $\bar{h}_s = V_s/A_s$ . In Fig. 5 (c) it can be observed that while initially the average thickness of the silicone oil liquid sheet is larger at atmospheric ambient pressure, eventually the influx of liquid cannot keep up with the spreading rate of the droplet and the average height decreases. This decrease in turn further limits the inflow of liquid, and the average height further declines till the liquid sheet breaks up.

#### IV. DISCUSSION

The simulations confirm the existence of a thin gas film at the edge of the spreading droplet<sup>6,26</sup>. A more in-depth analysis of the behavior of this gas film as function of different

material properties is found in Ref. 22. In this paper a closer look is taken at the properties of the gas film right before lamella formation and it is found that the simulations are able to reproduce the scaling of the gas film found in literature<sup>30</sup>. While the simulations presented in this work are performed in the continuum limit, the observed difference in the contact line velocity between atmospheric and reduced ambient pressure is consistent with the work of Sprittles<sup>11</sup>. Since Mandre, Mani, and Brenner<sup>6</sup> did not investigate subcontinuum effects in the gas film, this could provide an explanation of why they were not able to find a dependence of the gas film height on the ambient gas pressure. As shown in Fig. 4, the scaling of the lamella ejection time and the scaling of the lamella height as function of viscous and inertial forces is consistent with the work of Mongruel *et al.*<sup>5</sup>. This is in agreement with earlier work where we find a collapse of the data at the moment of lamella formation for a larger range of impact velocities<sup>22</sup>.

Unfortunately, the computational cost of these simulations make it unfeasible to perform simulations for a larger number of different viscosities: a simulation of a low viscosity ethanol splash takes several weeks and the simulation of a high viscosity silicone oil splash takes several months to complete. Therefore it was not possible to investigate the origins of the different trends which are observed when plotting the splashing threshold pressure as function of viscosity<sup>2,12,13</sup>. However, our observations concerning the thin gas film and lamella behavior are made for both low viscosity and high viscosity liquids. This confirms that the early time stages of droplet deposition are identical between high and low viscosity liquids and that thus conclusions reached from research on high viscosity liquids should also be valid for low viscosity liquids.

For late time spreading and breakup behavior of the droplets on the other hand significant differences are found. While at first glance the simulations do not seem to reproduce a crown splash, Fig 2 shows that in the case of a low viscosity liquid a very thin lamella forms right after impact and is ejected into the air at a high velocity. This causes a thicker air film to form under the liquid right away, and the lamella gets ejected as a liquid sheet. This behavior of the low viscosity liquid is also observed in experiments<sup>3</sup> and is consistent the idea of a lifting force acting on the liquid sheet<sup>7-9</sup>. As shown in Fig. 5 the liquid sheet for the high viscosity liquid forms in a different manner. A thick lamella becomes a thin liquid sheet due to limited inflow of liquid into the sheet. The identification of these two different types of liquid sheet formation and breakup is consistent with literature<sup>2,12,13</sup> and confirms that theories on splashing should take viscosity into consideration as an important parameter in their models.

## V. CONCLUSIONS

In this work simulations are presented of low viscosity ethanol and high viscosity silicone oil droplets impacting on a dry solid surface at atmospheric and reduced ambient pressure. To account for the liquid and gas phase the Volume Of Fluid (VOF) approach is used together with the Brackbill surface tension model<sup>16</sup> and the Generalized Navier Boundary Condition<sup>17,18</sup> to describe the surface tension and contact line behavior, respectively. The simulations are able to capture both the effect of the ambient gas pressure and liquid viscosity on droplet impact and breakup. The results suggests that the early time impact and gas film behavior for both low and high viscosity liquids share the same physics. However, for later time liquid sheet formation and breakup low and high viscosity liquids behave differently. A low viscosity lamella gets ejected into the air right after formation and becomes a liquid sheet. This is consistent with the idea of a lift force acting on the liquid<sup>7-9</sup>. A high viscosity liquid sheet on the other hand forms due to a limited inflow of liquid into the lamella/liquid sheet later in the spreading stage of the droplet. These results explain why for both kind of liquids the pressure effect can be observed, while at the same time different splashing regimes can be identified<sup>2,12,13</sup>. For future work we propose to closer investigate the transition between the low and high viscosity splashing regime to better understand the behavior of the threshold pressure as function of viscosity.

## ACKNOWLEDGMENTS

The authors would like to thank Sid Nagel and Andrzej Latka for many fruitful discussions and great insights.

## REFERENCES

- <sup>1</sup>A. L. Yarin, “Drop impact dynamics: splashing, spreading, receding, bouncing . . .,” *Annu. Rev. Fluid Mech.* **38**, 159–192 (2006).
- <sup>2</sup>C. S. Stevens, A. Latka, and S. R. Nagel, “Comparison of splashing in high-and low-viscosity liquids,” *Physical Review E* **89**, 063006 (2014).
- <sup>3</sup>L. Xu, W. W. Zhang, and S. R. Nagel, “Drop splashing on a dry smooth surface,” *Physical review letters* **94**, 184505 (2005).
- <sup>4</sup>A. Latka, A. Strandburg-Peshkin, M. M. Driscoll, C. S. Stevens, and S. R. Nagel, “Creation of prompt and thin-sheet splashing by varying surface roughness or increasing air pressure,” *Physical review letters* **109**, 054501 (2012).
- <sup>5</sup>A. Mongruel, V. Daru, F. Feuillebois, and S. Tabakova, “Early post-impact time dynamics of viscous drops onto a solid dry surface,” *Physics of Fluids (1994-present)* **21**, 032101 (2009).
- <sup>6</sup>S. Mandre, M. Mani, and M. P. Brenner, “Precursors to splashing of liquid droplets on a solid surface,” *Physical review letters* **102**, 134502 (2009).
- <sup>7</sup>G. Riboux and J. M. Gordillo, “Experiments of Drops Impacting a Smooth Solid Surface: A Model of the Critical Impact Speed for Drop Splashing,” *Physical Review Letters* **113**, 024507 (2014).
- <sup>8</sup>G. Riboux and J. M. Gordillo, “The diameters and velocities of the droplets ejected after splashing,” *Journal of Fluid Mechanics* **772**, 630–648 (2015).
- <sup>9</sup>G. Riboux and J. M. Gordillo, “Boundary-layer effects in droplet splashing,” *Physical Review E* **96**, 013105 (2017).
- <sup>10</sup>Y. Liu, P. Tan, and L. Xu, “Kelvin–Helmholtz instability in an ultrathin air film causes drop splashing on smooth surfaces,” *Proceedings of the National Academy of Sciences* **112**, 3280–3284 (2015).
- <sup>11</sup>J. E. Sprittles, “Kinetic effects in dynamic wetting,” *Physical Review Letters* **118**, 114502 (2017).
- <sup>12</sup>L. Xu, “Liquid drop splashing on smooth, rough, and textured surfaces,” *Physical Review E* **75**, 056316 (2007).
- <sup>13</sup>M. M. Driscoll, C. S. Stevens, and S. R. Nagel, “Thin film formation during splashing of viscous liquids,” *Physical Review E* **82**, 036302 (2010).
- <sup>14</sup>C. Hirt and B. Nichols, “Volume of fluid (VOF) method for the dynamics of free boundaries,” *Journal of computational physics* **39**, 201–225 (1981).
- <sup>15</sup>H. Rusche, *Computational Fluid Dynamics of Dispersed Two-Phase Flows at High Phase Fractions*, Ph.D. thesis, Imperial College (2002).
- <sup>16</sup>J. Brackbill, D. Kothe, and C. Zemach, “A continuum method for modeling surface tension,” *Journal of computational physics* **100**, 335–354 (1992).
- <sup>17</sup>T. Qian, X.-P. Wang, and P. Sheng, “Molecular scale contact line hydrodynamics of immiscible flows,” *Physical Review E* **68**, 016306 (2003).
- <sup>18</sup>J.-F. Gerbeau and T. Lelievre, “Generalized Navier boundary condition and geometric conservation law for surface tension,” *Computer Methods in Applied Mechanics and Engineering* **198**, 644–656 (2009).
- <sup>19</sup>E. Lauga, M. Brenner, and H. Stone, “Microfluidics: the no-slip boundary condition,” in *Springer handbook of experimental fluid mechanics* (Springer, 2007) pp. 1219–1240.
- <sup>20</sup>D. Jacqmin, “Contact-line dynamics of a diffuse fluid interface,” *Journal of Fluid Mechanics* **402**, 57–88 (2000).
- <sup>21</sup>O. Ltd, “OpenFOAM (Version 2.1.1) [Computer software],” (2011).
- <sup>22</sup>A. M. P. Boelens, A. Latka, and J. J. de Pablo, “Observation of the pressure effect in simulations of droplets splashing on a dry surface,” (2016), arXiv:1601.02134.
- <sup>23</sup>K. Kadoya, N. Matsunaga, and A. Nagashima, “Viscosity and thermal conductivity of dry air in the gaseous phase,” *Journal of physical and chemical reference data* **14**, 947–970 (1985).
- <sup>24</sup>A. M. P. Boelens and J. J. de Pablo, “Generalized navier boundary condition for a volume of fluid approach using a finite-volume method,” (2016), arXiv:1604.07880.
- <sup>25</sup>C. W. Visser, P. E. Frommhold, S. Wildeman, R. Mettin, D. Lohse, and C. Sun, “Dynamics of high-speed micro-drop impact: numerical simulations and experiments at frame-to-frame times below 100 ns,” *Soft Matter* **11**, 1708–1722 (2015).
- <sup>26</sup>J. M. Kolinski, S. M. Rubinstein, S. Mandre, M. P. Brenner, D. A. Weitz, and L. Mahadevan, “Skating on a film of air: drops impacting on a surface,” *Physical review letters* **108**, 074503 (2012).
- <sup>27</sup>J. Philippi, P.-Y. Lagr e, and A. Antkowiak, “Drop impact on a solid surface: short-time self-similarity,” *Journal of Fluid Mechanics* **795**, 96–135 (2016).
- <sup>28</sup>A. Latka, A. M. Boelens, S. R. Nagel, and J. J. de Pablo, “Drop splashing is independent of substrate wetting,” *Physics of Fluids* **30**, 022105 (2018).

- <sup>29</sup>R. Rioboo, M. Marengo, and C. Tropea, “Time evolution of liquid drop impact onto solid, dry surfaces,” *Experiments in fluids* **33**, 112–124 (2002).
- <sup>30</sup>S. Mandre and M. P. Brenner, “The mechanism of a splash on a dry solid surface,” *Journal of Fluid Mechanics* **690**, 148–172 (2012).